NANO · MICRO small
www.small-journal.com

Rapid Pressureless Sintering of Glasses

*Zhiwei Lin, Xinpeng Zhao, Chengwei Wang, Qi Dong, Ji Qian, Guangran Zhang, Alexandra H. Brozena, Xizheng Wang, Shuaiming He, Weiwei Ping, Gang Chen, Yong Pei, Chaolun Zheng, Bryson Callie Clifford, Min Hong, Yiquan Wu, Bao Yang, Jian Luo, Paul Albertus, and Liangbing Hu**

Silica glasses have wide applications in industrial fields due to their extraordinary properties, such as high transparency, low thermal expansion coefficient, and high hardness. However, current methods of fabricating silica glass generally require long thermal treatment time (up to hours) and complex setups, leading to high cost and slow manufacturing speed. Herein, to obtain high-quality glasses using a facile and rapid method, an ultrafast high-temperature sintering (UHS) technique is reported that requires no additional pressure. Using UHS, silica precursors can be densified in seconds due to the large heating rate (up to 10^2 K s^{-1}) of closely placed carbon heaters. The typical sintering time is as short as ≈10 s, ≈1–3 orders of magnitude faster than other methods. The sintered glasses exhibit relative densities of > 98% and high visible transmittances of ≈90%. The powder-based sintering process also allows rapid doping of metal ions to fabricate colored glasses. The UHS is further extended to sinter other functional glasses such as indium tin oxide (ITO)-doped silica glass, and other transparent ceramics such as Gd-doped yttrium aluminum garnet. This study demonstrates an UHS proof-of-concept for the rapid fabrication of high-quality glass and opens an avenue toward rapid discovery of transparent materials.

1. Introduction

Glasses, especially fused silica (SiO_2) glasses, are widely used in the fields of optics, electronics, and chemical manufacturing because of their extraordinary physicochemical properties, including high transparency, low thermal expansion coefficient, long-term chemical durability, good electrical insulation, and high hardness.[1–9] Conventionally, silica glasses are manufactured by melting natural crystalline quartz or silicon compound precursors at high temperatures from 2273 to 2573 K, followed by quenching. However, this traditional melting method requires a high energy input to reach the required temperature due to the high melting point of pure silica (≈2000 K). Conventional solid-state sintering can reduce the processing temperature but requires hours-long thermal treatment to obtain dense silica glasses.[10,11] It was reported that silica glass with a transmittance of ≈83% could be synthesized by gel-casting and sintering, in which the sintering temperature was reduced to 1373 K; however, the sintering time was still as long as 3 h.[12]

Recent studies have demonstrated new methods to synthesize silica glass, such as spark plasma sintering (SPS), flash sintering (FS), and laser sintering. SPS, also known as a field-assisted sintering technology, can obtain dense glasses with a short sintering time (e.g., 2–10 min) and a low-temperature range (e.g., 1073–1883 K).[13–16] However, SPS requires equipment to simultaneously provide mechanical pressure (e.g., 6–100 MPa) and high pulsed direct current, which could be costly for many commercial products.[13–16]

Z. Lin, X. Zhao, C. Wang, Q. Dong, J. Qian, A. H. Brozena, X. Wang, S. He, W. Ping, G. Chen, B. C. Clifford, M. Hong, L. Hu
Department of Materials Science and Engineering
University of Maryland
College Park, MD 20742, USA
E-mail: binghu@umd.edu

G. Zhang, Y. Wu
Kazuo Inamori School of Engineering, New York State College of Ceramics
Alfred University
New York 14802, USA

Y. Pei, C. Zheng, B. Yang
Department of Mechanical Engineering
University of Maryland
College Park, MD 20742, USA

J. Luo
Department of NanoEngineering
Program of Materials Science and Engineering
University of California San Diego
La Jolla, CA 92093, USA

P. Albertus
Department of Chemical and Biomolecular Engineering
University of Maryland
College Park, MD 20742, USA

L. Hu
Center for Materials Innovation
University of Maryland
College Park, MD 20742, USA

The ORCID identification number(s) for the author(s) of this article can be found under https://doi.org/10.1002/smll.202107951.

DOI: 10.1002/smll.202107951

Flash sintering, another rapid sintering technique, requires a high electric field (e.g., up to 3000 V cm^{-1}) due to the high electric resistivity of the glass powder compact.[17–20] Additionally, although the densification of the glass powders takes place within a few seconds during the FS process, the glass powders normally require long preheating in a conventional furnace, which substantially increases the overall processing time.[20] Laser sintering can quickly heat the silica precursors. However, the sintering rate is affected by the output power, scanning speed (e.g., 1 mm s^{-1}), and spot size (e.g., a diameter of ≈1 mm),[21] and the sintered porous structure results in low transparency.[22]

Currently, Joule heating and induction heating are introduced as advanced methods for rapidly synthesizing various materials such as graphene fiber,[23] phosphor converter,[24] and metastable 2D materials.[25] Recently, our group developed an ultrafast high-temperature sintering (UHS) method that can rapidly synthesize and sinter solid-state electrolytes,[26,27] metals,[28] phosphor converters,[29] and ceramics.[30,31] The challenge of sintering high-quality glasses with a facile and rapid method is now being addressed with UHS.

2. Results

2.1. Ultrafast Sintering of Glass in Seconds

Herein, we report a new strategy for glass manufacturing using rapid pressureless sintering to offer a different novel fabrication route. In a typical process, the SiO_2 powders are made into pellets by cold isostatic pressing (CIP) then placed in close contact with Joule-heated carbon heaters (i.e., carbon felt). The heaters can quickly reach temperatures of up to 1600 K, allowing the glass powder compact to be sintered to a dense glass in seconds via UHS (**Figure 1**a; and Figure S1, Supporting Information). During the UHS process, the Joule-heated carbon heater rapidly heats the pellet via thermal radiation and conduction. As shown in Figure 1b; and Figure S2, Supporting Information, the white pellet became translucent after CIP (40 MPa, 40 s), and then turned fully transparent and uniform after the UHS process. The UHS method can achieve 1–3 orders of magnitude faster sintering (Figure 1c) compared to other techniques such as gel-casting and sintering,[12] conventional furnace sintering,[10,11,32,33] SPS,[13–16] laser sintering,[22] and FS.[20] Compared with other sintering methods, our UHS technique has multiple advantages for glass fabrication. First, the large heating rate (≈10^2 K s^{-1}) and high sintering temperature (≈1600 K) of the carbon heater dramatically decrease the sintering time from hours to seconds. Dense and highly transparent silica glass can be rapidly sintered via the UHS method (Table S1, Supporting Information). Second, no applied pressure and relatively low current (< 50 A) enable a simple fabrication setup compared to other electrification methods such as SPS. Third, the UHS technique enables direct observation of the sintering process and allows for manual adjustment of the sintering temperature and time parameters in real-time. We further fabricated colored glasses with a simple solution-based doping process followed by our UHS sintering to kinetically trap in the doped elements. Beyond silica glass, our UHS method can potentially be extended to sinter a range of high-quality optical materials.

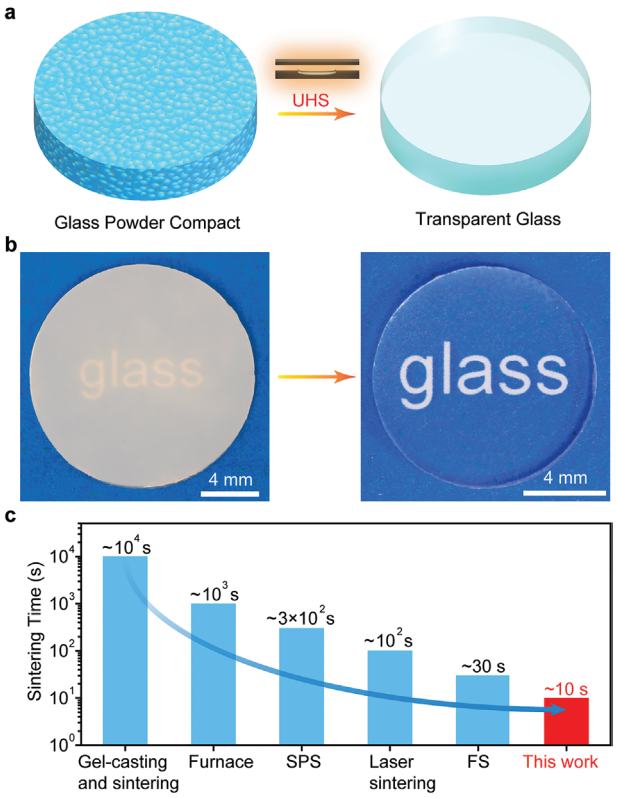

Figure 1. Ultrafast sintering of glass in seconds. a) Schematic of the UHS of dense and highly transparent glass from a glass powder compact. b) Optical images of the starting glass powder compact and the UHS sintered transparent pellet. c) Comparison of the typical sintering time with other solid-state sintering methods for bulk silica glass fabrication. Note that the sintering time of the FS does not include pre-heating (ramping) time in the furnace, which can be hours.

2.2. UHS Process for the Sintering of Glass

Amorphous silica nanoparticles with a mean particle size of 11 nm were used as the starting material to fabricate silica glass. A pressed pellet by the CIP process (40 MPa, 40 s) was placed in direct contact in the middle of the carbon heater for efficient heat transfer. In a typical UHS process for silica glass, the temperature applied to the pressed silica pellet is ramped up from room temperature (RT) to ≈1600 K in ≈10 s at a high heating rate of ≈10^2 K s^{-1} (**Figure 2**a; and Figures S3 and S4, Supporting Information). The pellet is then held isothermally at ≈1600 K for ≈10 s and rapidly cooled down at a cooling rate of up to ≈10^2 K s^{-1} by turning off the power source to the carbon heaters. During the ≈10 s sintering stage, we observed a fast volumetric shrinkage of the precursor pellet (Figure 2b), in which the silica glass shrank 28.7% in diameter (from 15.25 to 10.87 mm) and 27.9% in thickness (from 2.01 to 1.45 mm). This isotropic shrinkage can be attributed to the uniform sintering temperature and pressureless nature of the method. The sintering temperature can be easily controlled by adjusting the applied

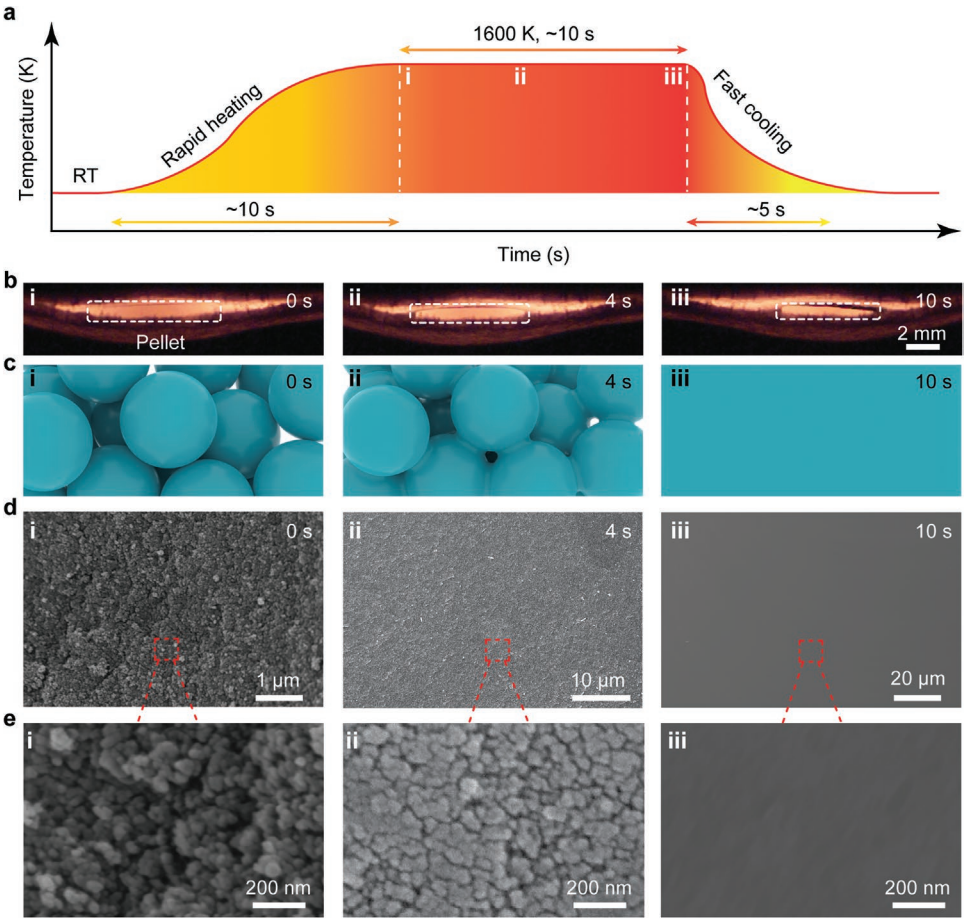

Figure 2. UHS process for the sintering of silica glass. a) A typical temperature profile of the UHS process for silica glass sintering. b) Optical images of the silica pellets in the carbon heater showing the fast shrinkage during the UHS process. c) Schematic illustrating the microstructural evolution during the UHS process. d) Cross-sectional SEM images and e) the corresponding magnified SEM images of the silica glass at different sintering times of (i) 0 s, (ii) 4 s and (iii) 10 s, respectively.

power for the carbon heater (Figures S5–S7, Supporting Information). The wide temperature range (300–3300 K) enables the UHS method to potentially be applied for rapid discovery and screening of other advanced glass materials (Figure S8, Supporting Information). The schematics (Figure 2c) and the corresponding cross-sectional scanning electron microscopy (SEM) images (Figure 2d,e) were applied to illustrate and study the evolution of the silica glass microstructure during the UHS process. Before the UHS process, the precursor pellet has a low relative density of ≈35% and was translucent, due to the uniformly distributed nanopores between the nanoparticles (Figure 2c–e,i). After sintering at ≈1600 K for ≈4 s, the nanoparticles begin to merge with neighboring nanoparticles, and the nanopores become smaller, decreasing the porosity with the relative density of ≈78% (Figure 2c–e,ii). At the final stage of the sintering process, a uniform and dense silica glass is acquired without any obvious pores or cracks (Figure 2c–e,iii), and the relative density increased to ≈98.4%, further demonstrating the ability of UHS to rapidly sinter dense silica glass. In addition, the X-ray diffraction (XRD) pattern revealed that the sintered silica glass features an amorphous structure (Figure S9, Supporting Information). We did not see carbon remnants on any samples after UHS treatment since there is no applied mechanical pressure (Figure S10, Supporting Information). Additionally, UHS can also utilize micro powder (≈44 μm) for silica glass fabrication with a relative density of > 98% (≈1600 K, ≈5 s) (Figure S11, Supporting Information). We tested the flexural stress of both a commercial glass slide and a UHS sintered glass using a three-point bending test (Figure S12, Supporting Information). The measured flexural stress of the sintered glass is ≈70 MPa, which is comparable with that of commercial float glass (≈58 MPa). The results indicate that the fast cooling does not undermine the mechanical properties of the sintered glass by UHS.

2.3. Optical and Thermal Performance of the Sintered Glass

To evaluate the transparency of the silica pellet before and after the UHS process, we measured the transmittance using ultraviolet–visible (UV–Vis) spectroscopy within the wavelengths ranging from 250 to 1000 nm. In the 250–350 nm range, the sintered glass exhibits low transmittance due to the absorption of light by silica, which is comparable to the results of both

float glass and silica aerogel.[34,35] However, for the unsintered pellet, because the size of the silica nanoparticles (≈11 nm) and the size of the gaps between neighboring nanoparticles are much smaller than the incident wavelength (250–1000 nm), the scattering of the light passing through the pellet is roughly described by Rayleigh scattering.[36] As such, we see that the transmittance of the pressed pellet before the UHS process increases with increasing wavelength (**Figure 3**a). In general, in the wavelength range of ≈400–1000 nm, the UHS sintered glass shows a higher transmittance (≈90%) than that of an unsintered pellet with the same thickness of ≈1.3 mm. After UHS, objects can be clearly viewed through the sintered glass, showing its high transmittance (Figure 3b).

Additionally, grid paper was used as the background for pictures to show the visual difference in transmittance (Figure 3c–f). The grid lines can be seen for both the pressed pellet and sintered glass when they are placed directly against the grid (Figure 3c,d). When the pellets are 3 cm above the grid, no grids can be observed for the pressed pellet, showcasing that the haze of the pressed pellet is large before the UHS process (Figure 3e). However, the lines can still be observed through the sintered glass due to its high transmittance. (Figure 3f). As illustrated in Figure 3g, pores in the pressed pellet before UHS can lead to Rayleigh scattering and contact resistance, which reduces the transmittance and thermal conductivity of the samples.[36–40] However, in the dense sintered silica glass, light and heat can directly transport through, resulting in a relatively higher transmittance or thermal conductivity. The pellet before the UHS process showed a lower thermal conductivity due to the extended heat transfer path caused by its porous structure

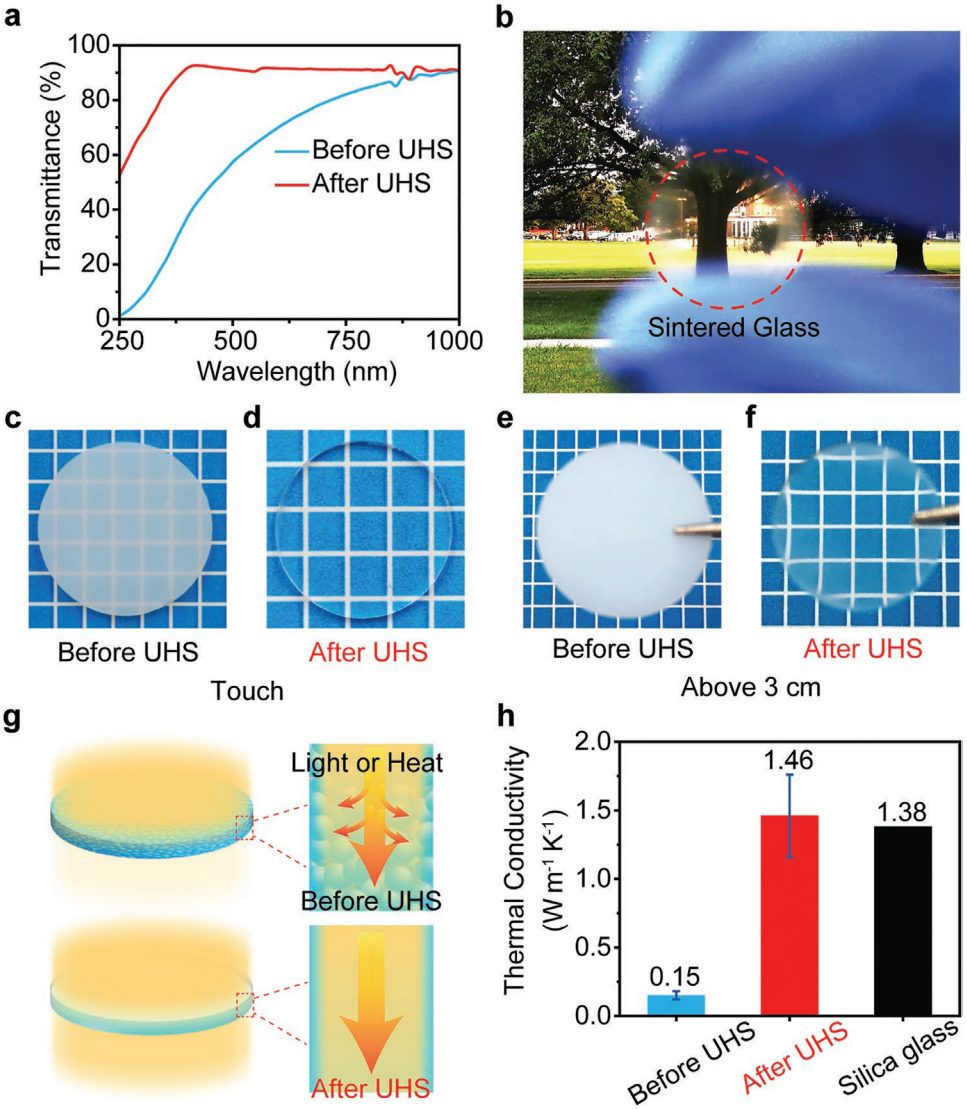

Figure 3. Optical and thermal performance of the sintered silica glass. a) Transmittance of the pellets before and after the UHS process. b) The optical image shows that the sintered glass has a high transmittance. c,d) The unsintered pellet and the UHS sintered glass when directly placed on a grid background, and e,f) when raised 3 cm above the grid background, demonstrating the difference in their transmittances. g) Schematics illustrating the transfer of light or heat through the porous glass pellet before sintering and the dense glass pellet after sintering. h) Comparison of the thermal conductivity of the pellets before and after the UHS process. Error bars show standard uncertainty. For reference, the thermal conductivity of fused silica glass is 1.38 $Wm^{-1}K^{-1}$ at room temperature.[41]

and the contact resistances between neighboring silica nanoparticles. According to our measurements, the sintered silica glass exhibited a thermal conductivity of ≈1.46 Wm^{-1} K^{-1}, which is comparable to the value of 1.38 Wm^{-1} K^{-1} for silica glass.[41] In contrast, the thermal conductivity of the pressed pellet was only ≈0.15 Wm^{-1} K^{-1}, ≈9 times lower than that of the sintered glass (Figure 3h). Such a large difference in transmittance and thermal conductivity resulted from the changes in the glass microstructure after the UHS process.

2.4. Optimization of the Sintering Conditions

To further explore the sintering mechanism of silica glass in the UHS process, we conducted detailed studies with different sintering parameters (i.e., time and temperature). All pellets were sintered in an inert Argon environment. First, we sintered pellets at a constant sintering temperature of ≈1600 K with varying sintering holding times ranging from 4 to 80 s (**Figure 4**a). It was found that when the sintering holding time was in the range of ≈8–20 s, dense silica glasses were sintered with high relative densities of > 98% (Figure 4b). As the sintering time increased to 50 s, the relative density decreased slightly to 95.1%; meanwhile, a small number of enclosed pores became observable via optical and SEM images. When the sintering time further increased (e.g., 80 s), the pores expanded to a size of tens of micrometers, leading to a lower relative density of sintered samples (Figure 4b; and Figure S13, Supporting Information). Argon is trapped before it is fully heated, i.e., the heat transport in SiO_2 bulk is faster than the heat transfer to Argon, such that Argon is still below the heater temperature before the pores become closed. As the temperature increases from 300 to 1600 K, the softness and fluidity of the silica glass increases, which reduces the interfacial tension between the entrapped gas and soft solid. Due to the high pressure of the trapped gas under a high-temperature environment, the volume of the entrapped gas increases, resulting in a decreased density. We attribute the round-like pores to the equilibrium of all local surface tensions of bubbles, indicating that the silica is in a highly-viscous glassy state.[42–45] Hence, the sintering holding time is an important parameter that affects the microstructure of the sintered pellet.

In addition, we studied the effect of sintering temperature on the sintered glass. At low temperature (e.g., 1300 K), even though the holding time was extended to 100 s, the pellet still did not become dense or transparent due to insufficient sintering, leading to a translucent material (Figure 4c; and Figure S14, Supporting Information). At higher temperatures (e.g., 1670 and 1750 K), a great number of enclosed pores were generated even at a shorter sintering time due to over-sintering (Figure 4d; and Figure S15, Supporting Information). Therefore, for sintering dense glasses, both low temperature and too high temperature should be avoided. With additional studies, we found that transparent silica glass could be readily sintered within a relatively wide range of sintering conditions (Figures S16 and S17, Supporting Information). The sintering conditions were plotted in a time-temperature diagram to demonstrate the appropriate conditions for achieving dense silica glasses (green area, ≈1600 K for 5–20 s, Figure 4e).

2.5. Demonstration of Functional Glasses Sintered Via UHS

To verify the feasibility of the UHS method in the application of functional glasses, multiple colored glasses were sintered via UHS. The simple powder-based sintering technique enabled us to dope the precursor material with metal ions in order to fabricate colored glasses for potential optical applications, such as optical filters.[46–50] **Figure 5**a shows the approach for sintering colored glasses, in which a solution of metal salt is pipetted and absorbed into the porous pressed pellet, followed by UHS. As shown in Figure 5b, the $FeCl_3$ ethanol solution-soaked pellet exhibited excellent transparency, indicating uniform absorption of the doping solution due to the capillary effect.[51] Homogeneous color distribution occurs since the uniform doping ions are kinetically trapped inside during the UHS process. This facile solution-based doping method can be applied to various metal salts to obtain different colored glasses. For example, blue, yellow, and red glasses were sintered via the UHS process at ≈1600 K in seconds by doping with solutions of $CoCl_2$, $FeCl_3$, and $CuCl_2$, respectively (Figure 5c,d). The metal salts may be transformed into oxides in the glass during the UHS process.[46,52] Taken together, these results demonstrate the unique capability of UHS to sinter modified glasses for additional optical properties with a solution-based doping method.

Furthermore, the UHS method was extended to fabricating other functional glasses such as those used in industrial, high-temperature applications. Commercial glass is not suitable for high-temperature applications because it is transparent to infrared light with a wavelength of 3–5 μm. To address this shortcoming, we designed a transparent glass composite, embedded with infrared plasmonic nanoparticles (e.g., indium tin oxide, ITO), to suppress thermal radiative losses by absorbing infrared thermal radiation (**Figure 6**a). The glass composite shows promising applications in concentrated solar power plants and observation windows for high-temperature chambers. To experimentally demonstrate this design, we doped 3 wt% ITO nanoparticles into silica powders, followed by UHS sintering (Figure 6b). The sintered functional glass obtained a relative density of > 98% (≈1600 K, ≈5 s), as shown in Figure 6c. Unlike the sintered pure silica glass, the 3 wt% ITO added glass, with a thickness of ≈1 mm, shows high infrared light absorption due to infrared plasmon resonances of the internal ITO nanoparticles (Figure 6d). The uniform distribution of the ITO nanoparticles occurs during the UHS process (Figure 6e–i). Note that the conventional method for making functional glass typically fabricates glass as the substrate, then follows with a coating process. Overall the conventional method has challenges: the functional layers on coating-based glasses are unable to sustain external mechanical stimulation (e.g., scratching or wiping), and the coating layers are easy to peel off at high temperature due to the thermal expansion mismatch between the coating layers and the glass substrate.[53,54] Fortunately, these issues can be avoided by our UHS method owing to the incorporation of ITO nanoparticles into the silica glass. We note that the low solar transmittance of sintered insulating glass is due to the high concentration of ITO nanoparticles. More work is needed in the future to optimize the concentration of ITO nanoparticles to achieve both high solar transmittance and low infrared transmittance

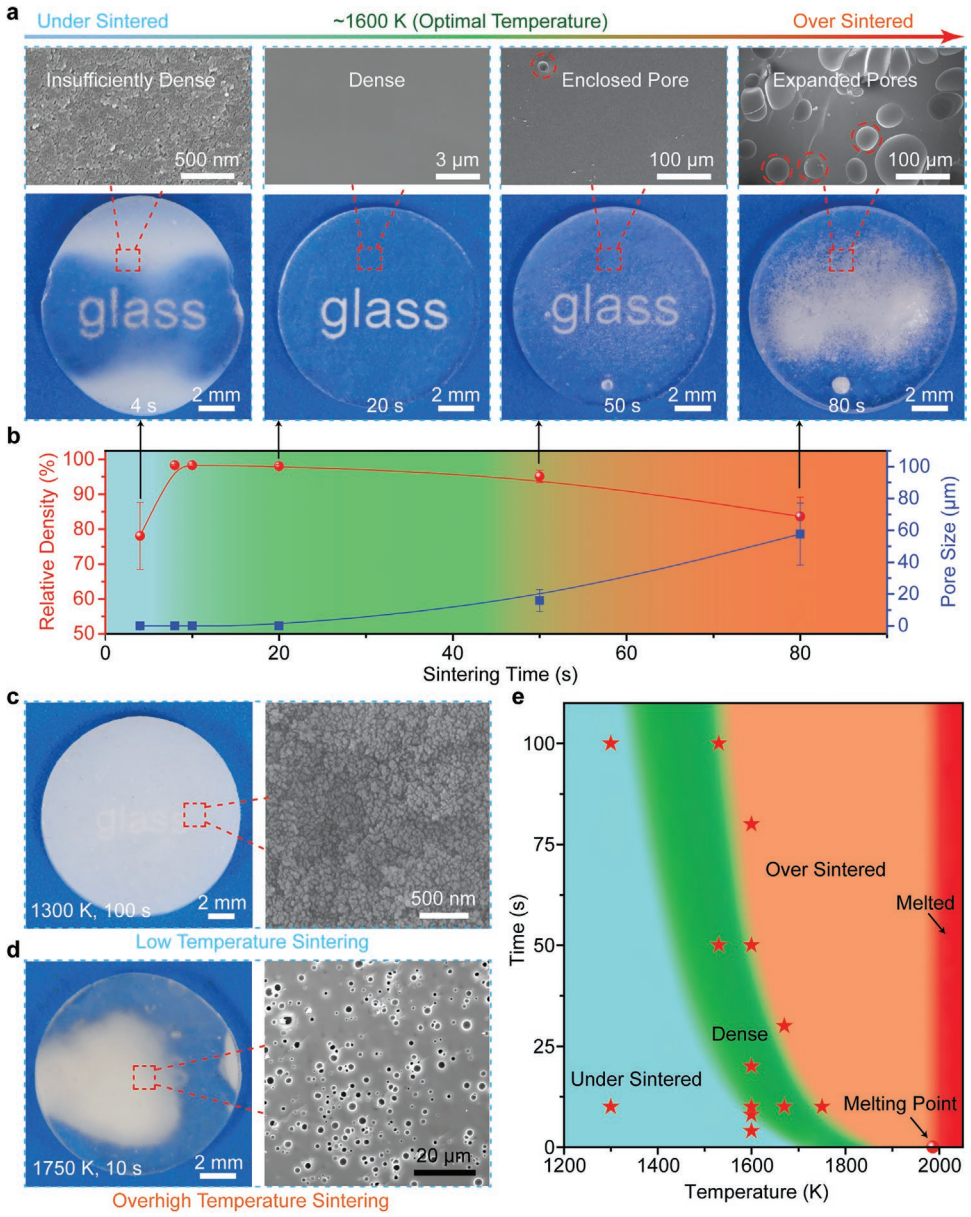

Figure 4. Optimization of sintering conditions, including sintering time and temperature. a) Optical and cross-sectional SEM images of the silica pellets sintered at ≈1600 K for various sintering times of 4 s, 20 s, 50 s, and 80 s. b) The relative density and pore size of the sintered glass as a function of the sintering time at ≈1600 K. Error bars show standard deviation. c) Optical image and cross-sectional SEM image of the silica pellet sintered at low temperature for a longer period of time (≈1300 K, 100 s). d) Optical and cross-sectional SEM micrographs of the silica pellet sintered at higher temperature for a short period of time (≈1750 K, 10 s). e) The time-temperature diagram for sintering silica glass, indicating the regions that are dense (green), porous without sufficient sintering (blue), porous with enclosed bubbles (brown), and melted (red).

(3–5 μm). Moreover, this pressureless sintering method can sinter glass with various shapes (Figure S18, Supporting Information). Our UHS method can also be applied to sinter other glass/amorphous materials and transparent ceramics with high quality and fast manufacturing speed. As shown in Figure S19, Supporting Information, we successfully sintered the transparent 1% Gd-doped yttrium aluminum garnet (YAG) with a relative density of ≈90% (i.e., 4.1 g cm^{-3}) via the rapid pressureless UHS process (≈2000 K, ≈30 min, ≈10^{-4} Torr). Silica-based compositions (e.g., 0.025 wt% ITO, 0.025 wt% MgO, and 0.025 wt% YAG, respectively) with relative densities of > 98% (≈1600 K, ≈5 s), were also successfully sintered as shown in Figure S20, Supporting Information.

3. Conclusion

In summary, we report a rapid and facile approach for sintering glasses to address the limitations of current sintering methods, such as long sintering times and complex manufacturing

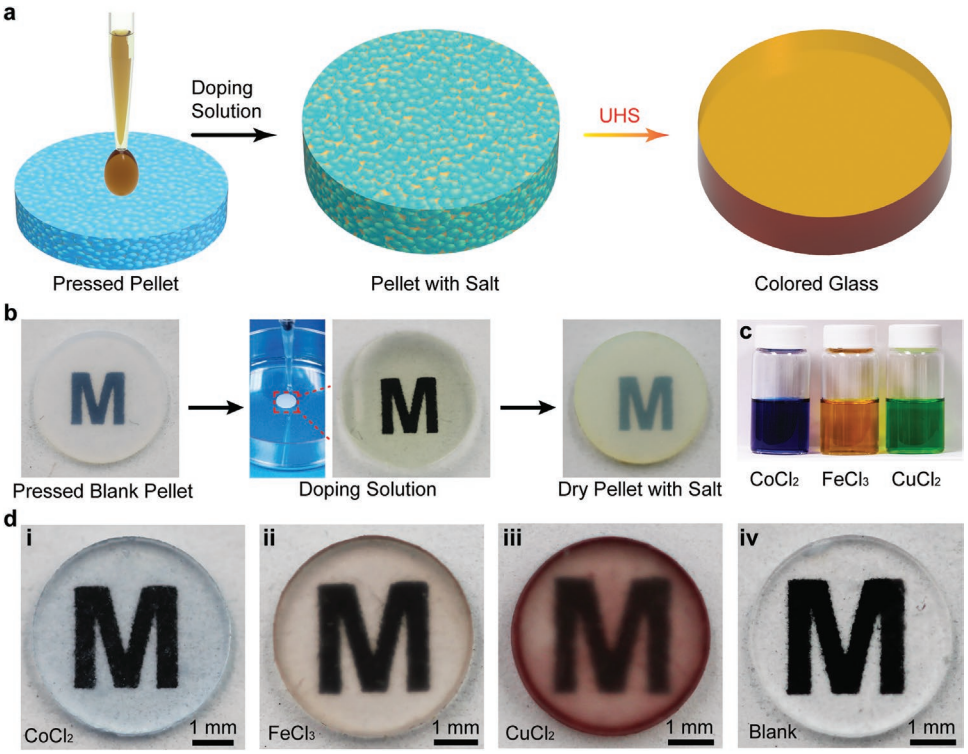

Figure 5. Demonstration of colored glasses sintered via UHS. a) Schematic indicating the fabrication process of the colored glasses by doping with metal salt solutions into the pressed pellets followed by the UHS process. b) Optical images showing the fabrication process of the metal-salt-infused pellet. c) Optical images of the various metal salt solutions, including $CoCl_2$, $FeCl_3$, and $CuCl_2$, and d) the corresponding colored silica glasses after sintering, which appear blue, yellow, and red. A glass without doping solution (blank) is also shown for comparison.

setup. The pressureless carbon-heater-based setup used to sinter glass powders features a simple configuration, and requires relatively low current of < 50 A (much lower compared to that of the SPS technique which is up to thousands of amperes). The UHS process simplifies the thermal treatment process by utilizing a large heating rate (up to $\approx 10^2$ K s^{-1}) to achieve a short sintering time. Notably, UHS sintering of glass reduces the general sintering time by 1–3 orders of magnitude compared to previous methods. The combination of starting nanoparticles and high heating rates that keep the sintering driving force high is the underlying mechanism of ultrafast sintering. The sintered silica glass features an optical transmission of ≈90% in a wide wavelength range of ≈400–1000 nm at 98.4% relative density. The optimal sintering time and temperature for achieving dense silica glasses were identified. The pressureless UHS method can be utilized to sinter various shapes of glass. Additionally, colored glasses were successfully fabricated by doping the pressed glass pellets with various metal salt solutions, followed by UHS at ≈1600 K in just seconds. We further extended the UHS method to other functional glasses and transparent ceramics, such as a glass composite embedded with infrared plasmonic nanoparticles (e.g., ITO) and Gd-doped yttrium aluminum garnet. The pressureless sintering method can not only be potentially integrated with a roll-to-roll process to realize continuous and scalable glass manufacturing but can also be applied for the discovery of other advanced glass materials for advanced optics, optoelectronics, and energy-efficient buildings.

4. Experimental Section

Materials Synthesis: Silica powder (99.8%, Sigma-Aldrich) with a particle size of ≈11 nm was used as a precursor for silica glass manufacturing by UHS. The silica powders were shaped into pellets using a pressing mold with diameters of 22 or 8 mm. Cold isostatic pressing was then applied to the pellets under a pressure of 40 MPa for 40 s to achieve a denser structure. For the doping experiments, 0.2 wt% cobalt(II) chloride hexahydrate ($CoCl_2{\cdot}6H_2O$, Sigma-Aldrich), 0.3 wt% iron(III) chloride hexahydrate ($FeCl_3{\cdot}6H_2O$, Sigma-Aldrich), and 0.15 wt% copper(II) chloride ($CuCl_2$, Sigma-Aldrich) were dissolved in ethanol. The pressed pellets were doped with these metal salt solutions by one-time soaking and dried in air for ≈10 min, followed by the UHS process to sinter the colored glasses. After the UHS process, the surfaces of the sintered specimens were carefully polished using abrasive paper (1200 fine grit). In addition, silica micro powder (99.5%, Sigma-Aldrich) with a particle size of ≈44 µm was also used for fabricating silica glass via UHS. Al_2O_3 (high purity alumina powder CR 10D, Baikalox), Y_2O_3 (99.999%, D_{50} = 3–5 µm, Stanford Advanced Materials), and Gd_2O_3 (99.9%, average particle size: 20–80 nm, Nanostructured & Amorphous Materials, Inc) were mixed according to the correct stoichiometric ratio. The mixed powder was milled with 0.4 wt% tetraethyl orthosilicate (Sigma-Aldrich) additive for 15 h. The suspension was then dried at 70 °C for 24 h. Finally, the powder was sieved with a 200-mesh grid and then was calcined at 1000 °C for 3 h. Thus, 1% Gd-doped YAG powder was prepared. The silica powder was mixed with proper 1% Gd-doped YAG powder, ITO powder (< 50 nm, Sigma-Aldrich), or MgO powder (≤ 50 nm, Sigma-Aldrich) to sinter the silica-based compositions.

Ultrafast High-Temperature Sintering Process: The UHS heater was made of a carbon felt heating strip (AvCarb Felt G200, ≈10 cm in length, ≈2 cm in width, and ≈3 mm in thickness). The center of the carbon felt heating strip was cut to sandwich the sample pellet. Next, the two

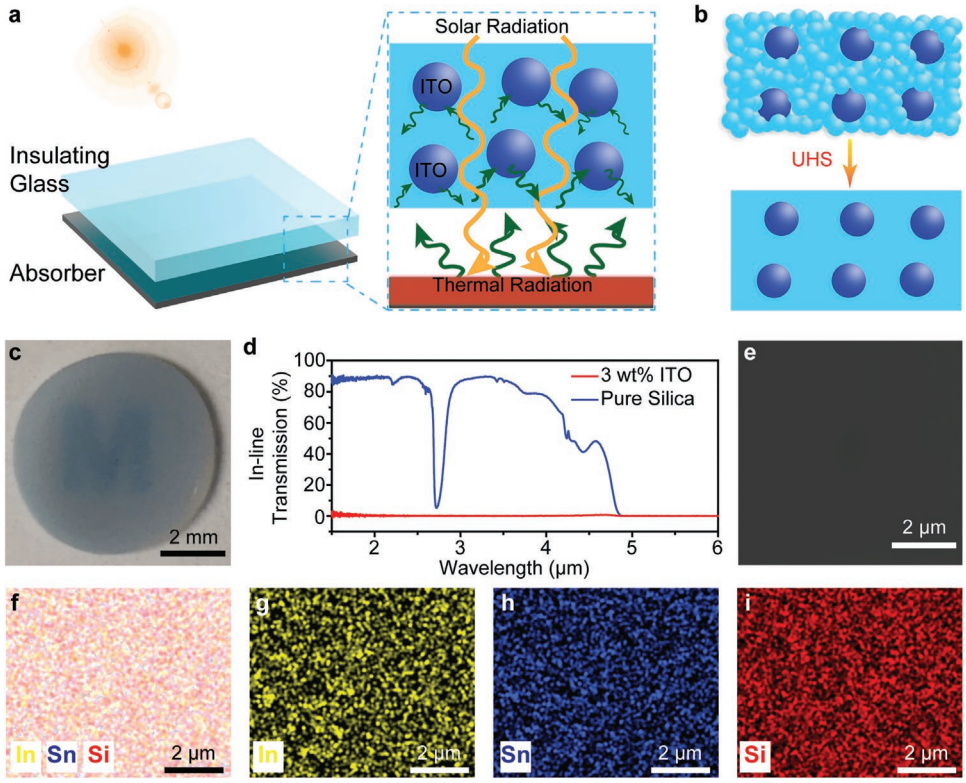

Figure 6. Demonstration of insulating glass sintered via UHS. a) Schematic of the insulating glass for high-temperature solar absorber, in which the infrared plasmonic nanoparticles (ITO) can absorb and re-emit thermal radiation, thus reducing the thermal radiative losses from the absorber. b) Schematic of the fabrication process of the insulating glass by incorporating ITO nanoparticles into silica glass with the UHS process. c) Optical image of the insulating glass sintered via UHS. d) In-line transmission of the insulating glass and pure silica glass. e) Cross-sectional SEM image of the insulating glass. f–i) EDX elemental mapping of the indium, tin, and silicon in the cross-section of the insulating glass.

ends of the carbon felt were fixed on two pieces of graphite sheets by clamps, respectively. The graphite sheets were connected to the outputs of an adjustable switch power supply (Star Power, 10050 DW) featuring tunable voltage and current (0–100 V and 0–50 A). The output power of the power supply can be adjusted to control the temperature of the carbon heater. In this manner, the CIP precursor pellets were sintered in an Ar-filled glovebox at different temperatures and times.

Material Characterization and Measurements: During thermal treatment, the temperature of the carbon heater was measured using a Vision Research Phantom Miro M110 high-speed camera with video recorded at 1000 frames s^{-1}, based on grey body radiation previously reported.[55] Calibration was performed by a Newport Oriel 67 000 Series Blackbody Infrared Light Source. Temperature estimations were made using color ratio pyrometry in which three color channels (red, green, and blue) are calculated and then matched to a gray-body calibration curve. The morphologies of the specimens were performed using a Tescan XEIA FEG SEM. A D8 Advanced (Bruker AXS, WI, USA) was used to analyze the XRD patterns of the samples with a scan rate of 5 ° min^{-1}. The transmittance was measured by a UV–Vis Spectrometer Lambda 35 from 250 to 1000 nm (PerkinElmer, USA). The flexural stress of the sintered glass and the commercial glass was measured with a 30 kN Instron Testing Machine. The support span was 20.5 mm. The dimensions of the sintered glass and the commercial glass for testing were 30.0 × 4.5 × 1.35 mm^3 and 30.0 × 5.46 × 1.00 mm^3, respectively. The in-line transmission in the infrared range was measured by Fourier-transform infrared spectrometer INVENIO (Bruker).

The thermal conductivity measurements were performed by a homemade laser-IR camera system and based on a steady-state method.[56] The prepared specimen was sandwiched between two aluminum blocks with a measured thermal conductivity of 206 Wm^{-1} K^{-1}. An aluminum pin fin heat sink was placed under the bottom aluminum block. To minimize the influence of the contact thermal resistance, thermal interface material (thermal grease, Shin Etsu X23-7783D) was applied to all contacting surfaces. A blue laser (465 nm Blue DPSS Laser) was used as the heat source, which was applied to heat the top aluminum block. A FLIR Merlin MID IR camera with a resolution of 320 × 256 pixels was used to capture the temperature distribution of the sample and aluminum blocks. When the laser-generated heat flux flowed through the sample from the top aluminum block to the bottom heat sink, a temperature difference occurred that was related to the thermal conductivity based on Fourier's law. The thermal conductivity was calculated based on a finite element model created with ANSYS which took radiative and convective heat loss into account.

Supporting Information

Supporting Information is available from the Wiley Online Library or from the author.

Acknowledgements

The authors acknowledge support from the University of Maryland A. James Clark School of Engineering. Y.W. acknowledges the support of the National Science Foundation (1554094). J.L. acknowledges the support of the Air Force Office of Scientific Research (Grant No. FA9550-19-1-0327).

Conflict of Interest

The authors declare no conflict of interest.

Author Contributions

Z.L., X.Z., and C.W. contributed equally to this work. L.H., Z.L., X.Z., and C.W. conceived the idea and designed the experiments. Z.L., X.Z., and C.W. sintered all samples. J.Q., W.P., G.C., and M.H. provided characterization via SEM and XRD. S.H. and G.Z. conducted the optical measurements. G.Z. and Z.L. prepared the glasses with various shapes before sintering. X.W., Q.D., and Z.L. performed the temperature measurements. Y.P., C.Z., and B.Y. measured the thermal conductivity. S.H. and Z.L. measured the flexural stress of the sintered glass and the commercial glass. L.H., Z.L., X.Z., C.W., Q.D., A.H.B., and B.C.C. collectively wrote the paper. All authors commented on the final manuscript.

Data Availability Statement

The data that support the findings of this study are available from the corresponding author upon reasonable request.

Keywords

functional glass, powder sintering, transparent materials, ultrafast high-temperature sintering

Received: February 11, 2022
Revised: March 9, 2022
Published online: March 30, 2022

[1] M. Ferrera, L. Razzari, D. Duchesne, R. Morandotti, Z. Yang, M. Liscidini, J. Sipe, S. Chu, B. Little, D. Moss, *Nat. Photonics* **2008**, *2*, 737.
[2] F. Kotz, N. Schneider, A. Striegel, A. Wolfschläger, N. Keller, M. Worgull, W. Bauer, D. Schild, M. Milich, C. Greiner, *Adv. Mater.* **2018**, *30*, 1707100.
[3] D. Zhang, W. Xiao, C. Liu, X. Liu, J. Ren, B. Xu, J. Qiu, *Nat. Commun.* **2020**, *11*, 2805.
[4] L. Wondraczek, J. C. Mauro, J. Eckert, U. Kühn, J. Horbach, J. Deubener, T. Rouxel, *Adv. Mater.* **2011**, *23*, 4578.
[5] A. Ikushima, T. Fujiwara, K. Saito, *J. Appl. Phys.* **2000**, *88*, 1201.
[6] S. Cheng, S. Schiefelbein, L. Moore, M. Pierson-Stull, C. Smith, S. Sen, *J. Non-Cryst. Solids* **2006**, *352*, 3140.
[7] J. Yao, L. Zhong, Z. Zhang, T. He, Z. Jin, P. J. Wheeler, D. Natelson, J. M. Tour, *Small* **2009**, *5*, 2910.
[8] D. X. Luong, K. V. Bets, W. A. Algozeeb, M. G. Stanford, C. Kittrell, W. Chen, R. V. Salvatierra, M. Ren, E. A. McHugh, P. A. Advincula, *Nature* **2020**, *577*, 647.
[9] A. Sinitskii, D. V. Kosynkin, A. Dimiev, J. M. Tour, *ACS Nano* **2010**, *4*, 3095.
[10] F. Kotz, K. Arnold, W. Bauer, D. Schild, N. Keller, K. Sachsenheimer, T. M. Nargang, C. Richter, D. Helmer, B. E. Rapp, *Nature* **2017**, *544*, 337.
[11] F. Kotz, P. Risch, K. Arnold, S. Sevim, J. Puigmartí-Luis, A. Quick, M. Thiel, A. Hrynevich, P. D. Dalton, D. Helmer, B. E. Rapp, *Nat. Commun.* **2019**, *10*, 1439.
[12] A. A. Al-Hasnawi, I. A. D. Al-Hydary, *Int. J. Appl. Eng. Res.* **2017**, *12*, 15257.
[13] J. Zhang, R. Tu, T. Goto, *Ceram. Int.* **2012**, *38*, 2673.
[14] T. G. Mayerhöfer, Z. Shen, E. Leonova, M. Edén, A. Kriltz, J. Popp, *J. Solid State Chem.* **2008**, *181*, 2442.
[15] D. Torikai, B. Barazani, E. Ono, M. Santos, C. Suzuki, *J. Aust. Ceram. Soc.* **2013**, *49*, 9.
[16] L. Wang, W. Jiang, L. Chen, Z. Shen, *J. Mater. Res.* **2009**, *24*, 3241.
[17] C. McLaren, W. Heffner, R. Tessarollo, R. Raj, H. Jain, *Appl. Phys. Lett.* **2015**, *107*, 184101.
[18] M. Biesuz, V. M. Sglavo, *J. Eur. Ceram. Soc.* **2017**, *37*, 705.
[19] M. Biesuz, W. D. Abate, V. M. Sglavo, *J. Am. Ceram. Soc.* **2018**, *101*, 71.
[20] M. O. Prado, M. Biesuz, M. Frasnelli, F. E. Benedetto, V. M. Sglavo, *J. Non-Cryst. Solids* **2017**, *476*, 60.
[21] J. Lei, A. A. Trofimov, J. Chen, Z. Chen, Y. Hong, L. Yuan, W. Zhu, Q. Zhang, L. G. Jacobsohn, F. Peng, *Opt. Mater.* **2017**, *68*, 63.
[22] N. K. Tolochko, M. K. Arshinov, K. I. Arshinov, A. V. Ragulya, *Powder Metall. Met. Ceram.* **2004**, *43*, 10.
[23] Y. Cheng, G. Cui, C. Liu, Z. Liu, L. Yan, B. Liu, H. Yuan, P. Shi, J. Jiang, K. Huang, *Adv. Funct. Mater.* **2021**, *32*, 2103493.
[24] Y. Peng, Y. Huang, Z. Lei, H. Wang, J. Liu, Y. Mou, M. Chen, *Mater. Today Commun.* **2021**, *29*, 102839.
[25] W. Chen, Z. Wang, K. V. Bets, D. X. Luong, M. Ren, M. G. Stanford, E. A. McHugh, W. A. Algozeeb, H. Guo, G. Gao, B. Deng, J. Chen, J. T. Li, W. T. Carsten, B. Yakobson, I, J. M. Tour , *ACS Nano* **2021**, *15*, 1282.
[26] C. Wang, W. Ping, Q. Bai, H. Cui, R. Hensleigh, R. Wang, A. H. Brozena, Z. Xu, J. Dai, Y. Pei, *Science* **2020**, *368*, 521.
[27] R. Wang, W. Ping, C. Wang, Y. Liu, J. Gao, Q. Dong, X. Wang, Y. Mo, L. Hu, *Adv. Mater.* **2020**, *32*, 2005059.
[28] C. Wang, W. Zhong, W. Ping, Z. Lin, R. Wang, J. Dai, M. Guo, W. Xiong, J. C. Zhao, L. Hu, *Adv. Sci.* **2021**, *8*, 2004229.
[29] Y. Liang, X. Ding, C. Yan, S. Bai, G. Liang, S. Yang, B. Liu, Y. Tang, *Opt. Express* **2021**, *29*, 14218.
[30] M. Kermani, D. Zhu, J. Li, J. Wu, Y. Lin, Z. Dai, C. Hu, S. Grasso, *Open Ceram.* **2022**, *9*, 100202.
[31] R.-F. Guo, H.-R. Mao, Z.-T. Zhao, P. Shen, *Scr. Mater.* **2021**, *193*, 103.
[32] O. Yong-Taeg, S. Fujino, K. Morinag, *Sci. Technol. Adv. Mater.* **2002**, *3*, 297.
[33] D. T. Nguyen, C. Meyers, T. D. Yee, N. A. Dudukovic, J. F. Destino, C. Zhu, E. B. Duoss, T. F. Baumann, T. Suratwala, J. E. Smay, *Adv. Mater.* **2017**, *29*, 1701181.
[34] X. Zhao, S. A. Mofid, B. P. Jelle, G. Tan, X. Yin, R. Yang, *Appl. Energy* **2020**, *278*, 115663.
[35] L. Zhao, S. Yang, B. Bhatia, E. Strobach, E. N. Wang, *AIP Adv.* **2016**, *6*, 025123.
[36] X. Zhao, S. Mofid, T. Gao, G. Tan, B. P. Jelle, X. Yin, R. Yang, *Mater. Today Phys.* **2020**, *13*, 100205.
[37] A. Ikesue, Y. L. Aung, *Nat. Photonics* **2008**, *2*, 721.
[38] Z. Xiao, S. Yu, Y. Li, S. Ruan, L. B. Kong, Q. Huang, Z. Huang, K. Zhou, H. Su, Z. Yao, W. Que, Y. Liu, T. Zhang, J. Wang, P. Liu, D. Shen, M. Allix, J. Zhang, D. Tang, *Mater. Sci. Eng., R* **2020**, *139*, 100518.
[39] Z. Lin, Y. Lan, C. Huang, *Int. J. Heat Mass Transf.* **2020**, *162*, 120340.
[40] H. Liu, M. Hu, J. Jiao, Z. Li, X. Wu, *Int. J. Heat Mass Transf.* **2020**, *161*, 120298.
[41] A. M. Hofmeister, A. G. Whittington, *J. Non-Cryst. Solids* **2012**, *358*, 1072.
[42] M. H. Ghatee, M. Zare, A. R. Zolghadr, F. Moosavi, *Fluid Phase Equilib.* **2010**, *291*, 188.
[43] G.-H. Zhang, K.-C. Chou, K. Mills, *ISIJ Int.* **2012**, *52*, 355.
[44] G.-H. Zhang, K.-C. Chou, Q.-G. Xue, K. C. Mills, *Metall. Mater. Trans. B* **2012**, *43*, 64.
[45] K. Cvecek, I. Miyamoto, M. Schmidt, *Opt. Express* **2014**, *22*, 15877.
[46] P. C. Schultz, *J. Am. Ceram. Soc.* **1974**, *57*, 309.
[47] X. Duan, D. Yuan, F. Yu, L. Wang, *Appl. Phys. Lett.* **2006**, *89*, 183119.
[48] X. Duan, D. Yuan, X. Cheng, X. Wang, Z. Wang, D. Xu, M. Lv, *Opt. Mater.* **2003**, *23*, 327.
[49] S. Mokhov, D. Ott, I. Divliansky, B. Zeldovich, L. Glebov, *Opt. Express* **2014**, *22*, 20375.

[50] L. Li, H. Lin, S. Qiao, Y. Zou, S. Danto, K. Richardson, J. D. Musgraves, N. Lu, J. Hu, *Nat. Photonics* **2014**, *8*, 643.
[51] S. He, C. Chen, Y. Kuang, R. Mi, Y. Liu, Y. Pei, W. Kong, W. Gan, H. Xie, E. Hitz, *Energy Environ. Sci.* **2019**, *12*, 1558.
[52] H. Wen, S. Xie, J. Cui, S. Mao, L. Luo, M. G. Brik, *J. Lumin.* **2019**, *213*, 263.
[53] P. Ashok, Y. S. Chauhan, A. Verma, *Opt. Mater.* **2020**, *110*, 110438.
[54] S. Sharma, S. Chaudhary, A. Kapoor, *J. Sol-Gel Sci. Technol.* **2017**, *82*, 315.
[55] R. J. Jacob, D. J. Kline, M. R. Zachariah, *J. Appl. Phys.* **2018**, *123*, 115902.
[56] T. Gao, Z. Yang, C. Chen, Y. Li, K. Fu, J. Dai, E. M. Hitz, H. Xie, B. Liu, J. Song, *ACS Nano* **2017**, *11*, 11513.